

## Impact of neutron irradiation on hardening of baseline and advanced tungsten grades and its link to initial microstructure

Yin, Chao; Terentyev, Dmitry; Dubinko, Andrii; Zhang, Tao; Wirtz, Marius; Antusch, Steffen; Petrov, Roumen H.; Pardoen, Thomas

**DOI**

[10.1088/1741-4326/abf417](https://doi.org/10.1088/1741-4326/abf417)

**Publication date**

2021

**Document Version**

Final published version

**Published in**

Nuclear Fusion

**Citation (APA)**

Yin, C., Terentyev, D., Dubinko, A., Zhang, T., Wirtz, M., Antusch, S., Petrov, R. H., & Pardoen, T. (2021). Impact of neutron irradiation on hardening of baseline and advanced tungsten grades and its link to initial microstructure. *Nuclear Fusion*, 61(6), Article 066012. <https://doi.org/10.1088/1741-4326/abf417>

**Important note**

To cite this publication, please use the final published version (if applicable).  
Please check the document version above.

**Copyright**

Other than for strictly personal use, it is not permitted to download, forward or distribute the text or part of it, without the consent of the author(s) and/or copyright holder(s), unless the work is under an open content license such as Creative Commons.

**Takedown policy**

Please contact us and provide details if you believe this document breaches copyrights.  
We will remove access to the work immediately and investigate your claim.

PAPER

## Impact of neutron irradiation on hardening of baseline and advanced tungsten grades and its link to initial microstructure

To cite this article: Chao Yin *et al* 2021 *Nucl. Fusion* **61** 066012

View the [article online](#) for updates and enhancements.



**IOP | ebooks™**

Bringing together innovative digital publishing with leading authors from the global scientific community.

Start exploring the collection—download the first chapter of every title for free.

# Impact of neutron irradiation on hardening of baseline and advanced tungsten grades and its link to initial microstructure

Chao Yin<sup>1,2,\*</sup>, Dmitry Terentyev<sup>1</sup>, Andrii Dubinko<sup>1</sup>, Tao Zhang<sup>3</sup>,  
Marius Wirtz<sup>4</sup>, Steffen Antusch<sup>5</sup>, Roumen H. Petrov<sup>6,7</sup> and  
Thomas Pardoën<sup>2</sup>

<sup>1</sup> Structural Materials Group, Institute of Nuclear Materials Science, SCK CEN, 2400 Mol, Belgium

<sup>2</sup> Institute of Mechanics, Materials and Civil Engineering, UCLouvain, 1348 Louvain-la-Neuve, Belgium

<sup>3</sup> Institute of Solid State Physics, Chinese Academy of Sciences, Hefei, Anhui 230031, China

<sup>4</sup> Forschungszentrum Jülich GmbH, Institut für Energie- und Klimaforschung, 52425 Jülich, Germany

<sup>5</sup> Karlsruhe Institute of Technology (KIT), Institute for Applied Materials, 76344

EGgenstein-Leopoldshafen, Germany

<sup>6</sup> Department of Electrical Energy, Metals, Mechanical Constructions & Systems, Ghent University, 9052, Ghent, Belgium

<sup>7</sup> Department of Materials Science and Engineering, Delft University of Technology, Delft, 2082, Netherlands

E-mail: [chaoyin@berkeley.edu](mailto:chaoyin@berkeley.edu) and [o33550110@gmail.com](mailto:o33550110@gmail.com)

Received 9 January 2021, revised 14 March 2021

Accepted for publication 31 March 2021

Published 29 April 2021



CrossMark

## Abstract

Six tungsten grades were irradiated in the Belgian material test reactor (BR2) and characterized by Vickers hardness tests in order to investigate the irradiation-induced hardening. These tungsten grades included: Plansee (Austria) ITER specification tungsten, ALMT (Japan) ITER specification tungsten, two products from KIT (Germany) produced by powder injection molding (PIM) and strengthened by 1% TiC and 2% Y<sub>2</sub>O<sub>3</sub> dispersed particles, and rolled tungsten strengthened by 0.5% ZrC from ISSP (China). The materials were irradiated face-to-face at three temperatures equal to 600 °C, 1000 °C, and 1200 °C to the dose of ~1 dpa. The Vickers hardness tests under 200 gf (HV0.2) were performed at room temperature. The Vickers hardness increases as the irradiation temperature increases from 600 to 1000 °C for all materials, except for the ZrC-reinforced tungsten, for which the increase of hardness does not depend on irradiation temperature. The irradiation-induced hardness decreases after irradiation at 1200 °C. This is a result of defect annealing enhanced by thermally activated diffusion. However, even at 1200 °C, the impact of neutron irradiation on the hardness increase remains significant; the hardness increases by ~30 to 60% compared to the non-irradiated value. In the case of TiC-strengthened material, the irradiation hardening progressively raises with irradiation temperature, which cannot be explained by the accumulation of neutron irradiation defects solely.

Keywords: tungsten, neutron irradiation, irradiation hardening, microindentation

(Some figures may appear in colour only in the online journal)

\* Author to whom any correspondence should be addressed.

## 1. Introduction

Tungsten is a mainstream candidate material for divertor and armor of plasma facing components (PFCs) owing to a high melting point, low erosion rate, and other attractive properties [1–3]. Although commercial ITER specification tungsten is available on the market, various particle reinforced grades and alloys from novel manufacturing processes have been recently developed to ease the machining process and/or to improve the low temperature mechanical properties and resistance against recrystallization at high temperature [4–6]. One of the novel manufacturing processes applicable for particle reinforced tungsten grades is the powder injection molding (PIM), which has the potential to be implemented for future divertor because of good industrial scalability potential and only limited post-machining requirements [7]. Another promising tungsten grade is reinforced with ZrC particles and processed by thermo-mechanical treatment (TMT). This ZrC reinforced tungsten grade is an attractive candidate since it has fine grain structure, low ductile to brittle transition temperature (DBTT), and improved microstructure stability at high temperature (i.e. resistance against recrystallization) [8–10].

During the nuclear phase of ITER operation and other magnetic confinement fusion devices, fast neutrons generated from the deuterium–tritium (D–T) nuclear fusion reaction will degrade the mechanical properties of PFCs materials. Moreover, the divertor PFCs based on the tungsten monoblock design will also be exposed to high-heat-flux during normal operation. This high flux of low energy plasma ions causes erosion and thermal loads (inducing thermo-mechanical stresses), which eventually cause cracking phenomena at the surface of the plasma-facing divertor components [11]. Furthermore, fast neutrons penetrate deep in the bulk and cause degradation of the bulk properties. The studies by Hasegawa *et al* and Fukuda *et al* focused on irradiation hardening and microstructural evolution induced by neutron irradiation produced by various test reactors (HFIR, JOYO, and JMTR) in tungsten alloys [12–15] and in other advanced tungsten grades [16]. Their results show that the composition of the tungsten alloys and the addition of strengthening particles affect the resistance to the irradiation hardening. For instance, in tungsten alloyed with Re and in ultra-fine grain tungsten reinforced by TiC, the resistance against the irradiation hardening increases, whereas in tungsten alloyed with La, the resistance to irradiation hardening decreases at doses lower than 0.5 dpa. Moreover, the density of irradiation-induced defects like voids, dislocation loops, and precipitates vary with irradiation conditions (i.e. irradiation temperature and dose). Since each type of irradiation-induced defect has its unique contribution to the overall irradiation hardening [17], a tungsten grade with different defect populations will exhibit different mechanical performance. Therefore, investigating the high temperature neutron irradiation effects at higher irradiation temperature on tungsten grades produced with the above mentioned novel manufacturing processes is absolutely necessary in order to understand their potential resistance to irradiation damage under different irradiation conditions. This knowledge can assist industry to develop new types of irradiation resisting tungsten alloys, and

engineers can implement the new tungsten alloys to optimize the design of PFCs, offering durable and safe operation in the nuclear fusion environment.

In this work, we perform a parametric study addressing the effect of high temperature neutron irradiation on the hardness change in two types of particle reinforced tungsten and compare them to several tungsten grades, which includes the results from the same campaign already published in reference [18]. The neutron irradiation is performed over a wide range of temperatures, being relevant to the ITER operational conditions. The samples made of different materials are irradiated face-to-face to ensure equivalent irradiation history, thus enabling a comparative study. The hardness of reference and as-irradiated samples is measured using Vickers hardness indentation at room temperature.

## 2. Experimental procedures

### 2.1. Materials

Six different tungsten grades are investigated. The materials can be categorized into two groups: commercial pure tungsten grades (also called ITER baseline grades) and particle reinforced grades. The three ITER baseline grades are ITER specification tungsten materials produced by Plansee (henceforth referred to as IGP), recrystallized IGP tungsten (henceforth referred to as W-RX, also known as IGP-RX in our previous work [18]), and ITER specification tungsten produced by A.L.M.T. (henceforth referred to as IGA, also known as ALMT in our previous work [18]). The W-RX is produced by heating up the IGP to 1600 °C and holding this temperature for 1 h in a protective hydrogen atmosphere. The other tungsten products are particle reinforced grades, namely: tungsten alloyed with 0.5 wt% of ZrC (henceforth W0.5ZrC), tungsten alloyed with 1 wt% of TiC (henceforth W1TiC), and tungsten alloyed with 2 wt% of Y<sub>2</sub>O<sub>3</sub> (henceforth W2YO). W0.5ZrC material is produced by the Institute of Solid State Physics, China, and supplied as a plate product, which is sintered at 2200 °C under a pressure of 70 MPa for 20 h in vacuum, followed by rolling and TMT. Both W1TiC and W2YO are produced by PIM techniques (sintered at 2400 °C) by Karlsruhe Institute of Technology, Germany. Table 1 summarizes the composition of these tungsten grades. In the upcoming sections results and discussion, table 2 summarizes the main characteristics of these six materials.

### 2.2. Microstructure

A scanning electron microscope equipped with energy-dispersive x-ray spectroscopy (EDS) and electron back-scattered diffraction (EBSD) systems is employed for microstructural characterization. In order to perform chemical composition analysis, the samples are finally ground with P4000 SiC paper. After grinding with P4000 SiC paper, additional electropolishing is applied to the final surface just before the EBSD scan for the EBSD analysis. The electrolyte for electropolishing is 1.5 wt% NaOH solution, and the parameters are 25 V with a flow rate of 18 L min<sup>-1</sup> in the mask area of 2 cm<sup>2</sup>

**Table 1.** Composition of the tungsten grades (the main composition is provided by the manufacturers, and the impurities of pure tungsten can be referred to [19]). More information on the composition of W-0.5ZrC and PIM tungsten grades can be found in [7, 8], respectively. The tungsten grades in the literature and investigated here were produced by the same manufacturing process and institute/company.

Materials	Main composition (weight)	Impurities of pure W (ppm in weight)					
		Cr	O	Cu	Fe	Ni	Mo
<b>IGP</b>	>99.97% W	1.1	13	3.4	5.2	0.4	5.1
<b>IGA</b>	>99.99% W	0.3	8	0.4	1.4	0.4	0.7
<b>W0.5ZrC</b>	99.5% W + 0.5% ZrC	—	—	—	—	—	—
<b>W-RX</b>	>99.97% W	1.1	13	3.4	5.2	0.4	5.1
<b>W1TiC</b>	99% W + 1% TiC	—	—	—	—	—	—
<b>W2YO</b>	98% W + 2% Y <sub>2</sub> O <sub>3</sub>	—	—	—	—	—	—

**Table 2.** Dimensions of the grains and of the strengthening particles of different tungsten grades.

Materials	Equivalent diameter ( $\mu\text{m}$ )							
	Plane normal to	W Grain			Particle			
		D10	D50	D90	D10	D50	D90	
<b>IGP</b>	ND	14.5	52.7	103.9	—	—	—	
	LD	4.8	15.8	31.5	—	—	—	
	ND	5.9	19.5	41.0	—	—	—	
<b>IGA</b>	LD	4.3	9.9	19.2	—	—	—	
	ND	1.9	4.5	9.2	0.2	0.4	0.8	
<b>W0.5ZrC</b>	LD	1.4	2.8	5.5	—	—	—	
<b>W-RX</b>	—	31.7	60.4	108.4	—	—	—	
<b>W1TiC</b>	—	1.8	6.0	9.8	0.4	0.9	1.6	
<b>W2YO</b>	—	2.2	6.2	11.8	0.6	1.2	2.0	

for 1 min at room temperature. The grain size, grain orientation, and grain boundary misorientation angles are identified by analyzing the EBSD data using EDAX-TSL OIM analysis software. The equivalent 10% diameter (D10), equivalent medium diameter (D50), and equivalent 90% diameter (D90) of grains are identified, where D10, D50, and D90 indicate that there are 10%, 50%, and 90% (in area fraction) of the grains or particles smaller than this diameter, respectively. Therefore, the grain size distribution of each tungsten grade can be evaluated based on D10, D50, and D90 values. The particle identification procedure is implemented by combining back-scattered electron (BSE) signal and EDS mapping. The particle size is analyzed using the ImageJ software. As will be shown later, the hardness of the materials is linked to the size and shape of the grains. This is not surprising given that the hardness is linked to the ability of the material to accommodate the external load into elastic and plastic deformation. In the general case of equiaxed grains, the yield stress is proportional to  $D^{-1/2}$  ( $D$  is grain size) as expected from Hall–Petch relationship. Given that some of the studied materials exhibit non-equiaxed grains, we have used EBSD data to find a rigorous mathematical relationship between the grain size/shape parameters and Vickers hardness. The basic idea is to link the Vickers hardness with the linear density of interfaces (i.e. grain boundary or precipitate interface), which are inversely proportional to grain size (or precipitate size) and expected to obstruct plastic deformation

(and therefore contribute to the hardness) [20]. The analysis performed here is mainly based on the results of the EBSD and EDS measurements of the reference microstructure. As will be discussed in the results section, the present work would very much benefit from a detailed microstructural study of the neutron irradiated samples by employing EBSD and transmission electron microscopy (TEM). However, this is currently impossible to perform due to the very high residual activity of the samples (well exceeding  $50 \text{ mSv h}^{-1}$ , so that even cutting the samples into smaller pieces would not resolve the activation issue). Further cooling is required to proceed with the preparation of the samples for the microstructure investigation of as-irradiated materials. The next paragraph provides a brief explanation of the quantification of the linear density of the interfaces.

In general, the shape of an elongated grain of the rolled/forged tungsten grade can be well approximated by an ellipsoid, as shown in figure 1.  $A$  and  $B_1$  are the major and minor medium length values (in area fraction) given the projection of a grain on a plane perpendicular to the normal direction (ND).  $B_2$  and  $C$  are the major and minor medium length values for the projection on a plane normal to the longitudinal direction (LD). The meaning of  $A$ ,  $C$ ,  $B_1$ , and  $B_2$  can be easily understood from figure 1. These measurements are analyzed using the EDAX-TSL OIM software, where the minimum number of pixels required to define a grain is 2, and

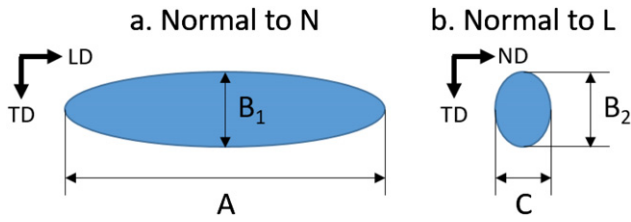


**Figure 1.** The projected shape of an ellipsoidal grain on (a) plane normal to ND and (b) plane normal to LD.

the minimum misorientation angle of  $2^\circ$  is selected for all the grains, including sub-grains, and  $15^\circ$  is applied for grains with high angle grain boundaries (HAGBs). The volume ( $V_e$ ), the approximated surface area ( $A_e$ ) [21, 22], and the grain boundary surface area to volume ratio ( $S_v$ ) of the ellipsoidal grain can be described as follows,

$$V_e = \frac{4}{3}\pi ABC, \quad (1)$$

$$A_e = 4\pi \left( \frac{A^p B^p + A^p C^p + B^p C^p}{3} \right)^{1/p}, \quad (2)$$

$$S_v = \frac{A_e}{2V_e}, \quad (3)$$

where  $p$  is a constant equal to 1.6075 [23], which gives a relative error of 1.061% in area. From the geometrical considerations,  $B$  should be equal to both  $B_1$  and  $B_2$ ;  $B$  is taken as the arithmetic mean value of  $B_1$  and  $B_2$ .

The  $S_v$  of equiaxed grains can be described as follow,

$$S_v = \frac{3}{D50}, \quad (4)$$

where D50 is the equivalent medium diameter of the grains. The  $S_v$  of grains or sub-grains with a misorientation angle larger than  $2^\circ$  ( $S_{v,iG}$ ) can be defined as the total  $S_v$  of sub-grains ( $S_{v,SG}$ ) and grains ( $S_{v,G}$ ) where sub-grains and grains are surrounded by low angle grain boundaries (LAGBs) with misorientation between  $2$  to  $15^\circ$  and HAGBs with a misorientation angle larger than  $15^\circ$ , respectively. Therefore,  $S_{v,SG}$  can be calculated as:

$$S_{v,SG} = S_{v,iG} - S_{v,G}. \quad (5)$$

Contrary to grain boundaries, the strengthening particles do not share common interfaces, and therefore the  $S_v$  of strengthening particles,  $S_{v,p}$  (i.e. valid for W1TiC, W2YO, and W0.5ZrC), is defined as:

$$S_{v,p} = \frac{6}{D50}. \quad (6)$$

### 2.3. Neutron irradiation

The disk specimens are irradiated in the Belgian reactor (BR2). BR2 is a type of materials testing reactor with flexibility to utilize the reactor core configuration and operation mode to adapt the requirements of experiment in terms of fast and thermal neutron flux. The specimens are placed in the 1.5 mm thick

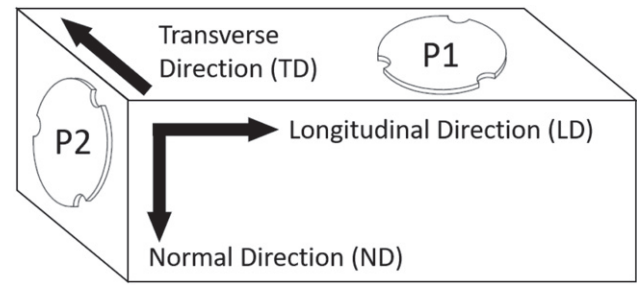


**Figure 2.** Sampling scheme for disk samples.

stainless steel capsule filled with inert gas to prevent oxidation. The stainless steel capsule also acts as a shield to avoid extensive transmutation. The typical transmutation rate was about 2 at.%Re/dpa, which otherwise would be a factor of 5 higher. The position of the specimens inside the capsule is secured by centering using  $Al_2O_3$  holders, spacers and guiding rods in order to maintain the dedicated gap between the stack of specimens and inner capsule wall to achieve the required irradiation temperature. Such design has been already applied in a number of recent experiments carried out on tungsten and tungsten alloys, more details are available in [24–26]. The capsules are embedded inside the fuel element, where the fast neutron ( $E > 0.1$  MeV) flux is  $7 \times 10^{14}$  n cm $^{-2}$  s $^{-1}$  at a reactor power of 60 MW. The calculation of the irradiation dose in displacement per atom (dpa) units is performed by MCNPX 2.7.0 [27] for the threshold displacement energy of 55 eV. The irradiation doses and temperatures on the samples are found to be 0.95 dpa at 600 °C, 1.00 dpa at 1000 °C, and 1.13 dpa at 1200 °C using the MCNP calculations (neutron flux, gamma flux, heat release due to prompt and delayed gamma and neutron heating), reactor power measurements, and finite element thermal calculations (the irradiation temperatures are nominal values calculated as average during the cycle). During the reactor cycle, the actual temperature on the samples exhibits an excursion of about  $\pm 5\%$  with respect to the nominal value. The ALEPH code of SCK CEN [28] and accessible nuclear databases [29–31] are applied for the calculation of transmuted elements. The summed concentration of transmuted Re and Os for 0.95 dpa, 1.00 dpa, and 1.13 dpa is 1.80 at.%, 1.96 at.%, and 2.13 at.%, respectively. The transmutation of ZrC is assessed based on the comparison of pure tungsten and tungsten with 1 wt% ZrC (referred as W1ZrC) for a dose of 1 dpa using the BR2 fuel channel (i.e. relevant for this work) and the DEMO first wall neutron spectrum. The result indicates that there is no major difference in terms of transmutation products between the two grades in the BR2 spectrum (only a negligible amount of Zr,  $\sim 4$  appm, is transmuted in W1ZrC). In terms of gas production, the addition of C will promote the formation of He in DEMO spectrum from  $\sim 0.5$  appm for pure tungsten to 7.3 appm for W1ZrC alloy. However, in the BR2 spectrum, the effect of ZrC in terms of the formation of He is negligible. The confirmation of the concentration of transmuted elements requires further investigation by compositional analysis. Currently, such analysis cannot be performed yet due to high residual activity of the samples (exceeding 10 mSv h $^{-1}$ ).

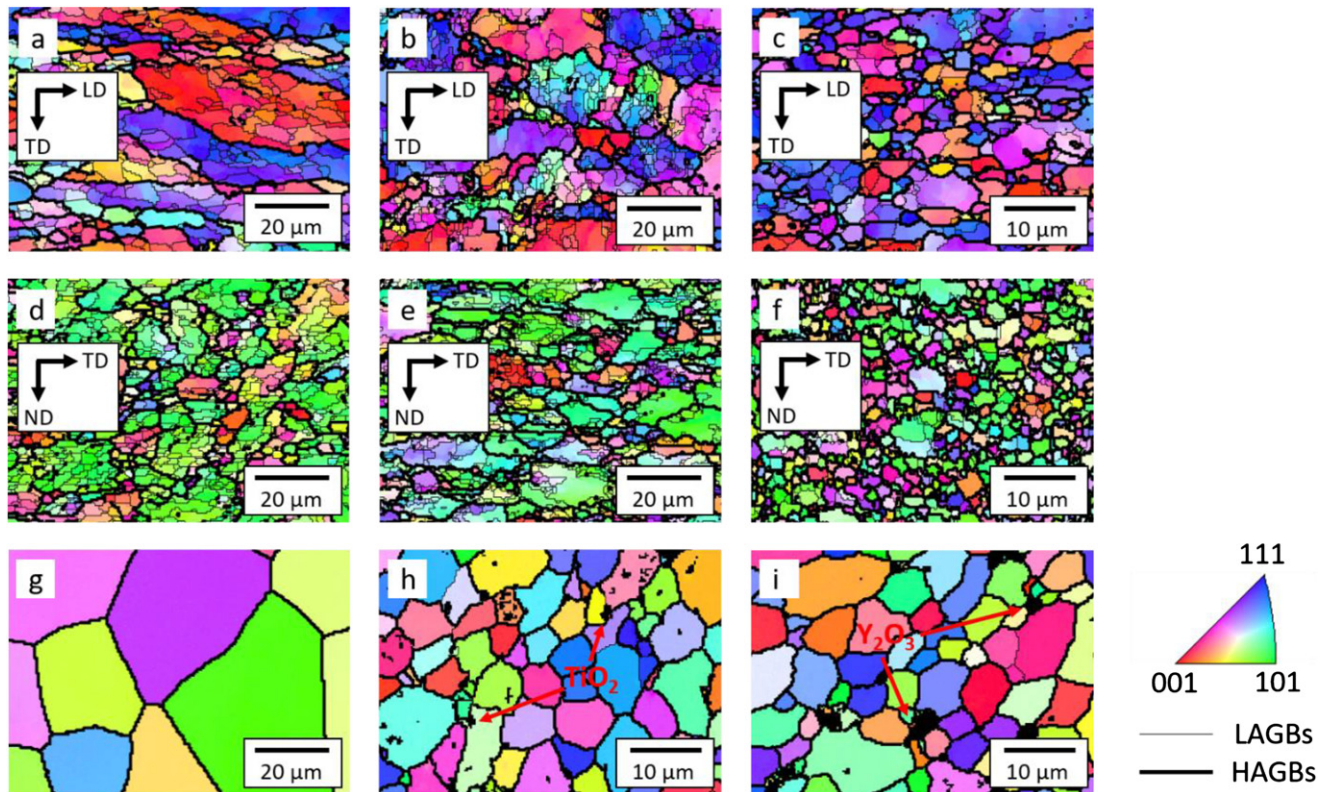


**Figure 3.** Inverse pole figure of tungsten grades showing LAGBs and HAGBs interfaces. (a) IGP plane normal to ND; (b) IGA plane normal to ND; (c) W0.5ZrC plane normal to ND; (d) IGP plane normal to LD; (e) IGA plane normal to LD; (f) W0.5ZrC plane normal to LD; (g) W-RX; (h) W1TiC; (i) W2YO.

#### 2.4. Micro-hardness test

The specimens for micro-hardness tests are disks with a diameter of  $\sim 12$  mm and 0.5 mm in thickness. The two sampling orientations for the disks are shown in figure 2. The final surface undergoing the indentation is polished with P2000 SiC paper or higher grit before irradiation. No sample preparation was applied after the irradiation. The micro-hardness test is performed by Vickers indentation under a force of 200 gf inside the shielded hot cell operated by remote manipulators at room temperature. The time to reach the maximum force and the hold time is 10 s each. ASTM standard E384 is referred for the calculation of Vickers hardness (HV, with a unit of GPa). In order to generate statistically reliable data, up to nine indents are made on each specimen in different areas around the center of the disk. The hardness tests are performed on the plane orthogonal to ND for W0.5ZrC (as demonstrated in figure 2, P1 disk) and on the plane orthogonal to LD for IGP and IGA grades (as demonstrated in figure 2, P2 disk). This choice is made because the plane of IGP and IGA (orthogonal to LD) will correspond to the side of the PFCs facing the plasma beam in the Tokamak. This plane, selected to face the plasma, has been chosen to prevent grain debonding on the tungsten surface (expected to result from the crack deflection), which would lead to contamination of the plasma. Differently from IGP and IGA, the preference plasma facing plane for W0.5ZrC is not decided yet. Moreover, the grain size of W0.5ZrC is much smaller than that of the two commercial tungsten grades, and thus the anisotropy

of hardness (depending on the indented plane) is much smaller. Therefore, the plane orthogonal to ND is selected for W0.5ZrC to perform hardness tests in this work since manufacturing the samples is easier for this orientation.

### 3. Results and discussion

#### 3.1. Microstructure

Figure 3 shows the microstructure represented by inverse pole figures for the different tungsten materials. The thick black lines and thin black lines indicate, respectively, the HAGBs (with misorientation  $> 15^\circ$ ) and LAGBs (with misorientation between 2 to  $15^\circ$ ). HAGBs and LAGBs can also be described as boundaries between grains and sub-grains, respectively. As shown in figures 3(a) and (d), the grains of IGP are elongated in the LD. Since the width of the grain along the ND and transverse direction is small, one can describe the shape of IGP grains as carrot-like bodies. The grain shape of W-RX is shown in figure 3(g). The elongated carrot-like grains of IGP have evolved towards equiaxed grains after recrystallization. Differently from IGP, the grains of both IGA and W0.5ZrC exhibit a pancake-like shape with a major axis parallel to LD, as shown in figures 3(b), (c), (e) and (f). However, the grain size of W0.5ZrC is much smaller than that of IGA because of the TMT applied to W0.5ZrC [8]. The PIM manufacturing process did not include any mechanical post-treatment, and therefore W1TiC and W2YO products have equiaxed shaped grains.

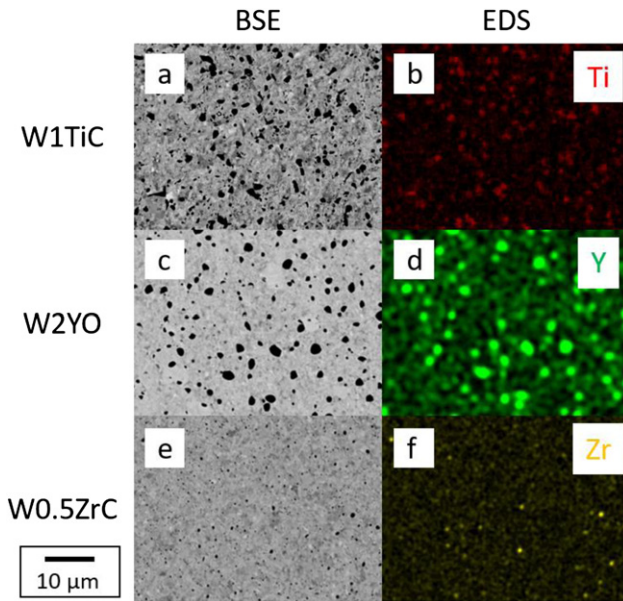


**Figure 4.** BSE image and EDS map of particle reinforced tungsten grades. (a) BSE and (b) EDS of W1TiC; (c) BSE and (d) EDS of W2YO; (e) BSE and EDS of W0.5ZrC. Red, green, and yellow colors indicate elements of Ti, Y, and Zr, respectively.

The strengthening particles in W1TiC, W2YO, and W0.5ZrC grades are homogeneously distributed in the matrix, as shown in figure 4. D50, D10, and D90 values for the grains and the strengthening particles are given in table 2.

As shown in table 3, the medium length of the major axis and minor axis of the grains and sub-grains are measured for IGP, IGA, and W0.5ZrC in the planes normal to ND and LD in order to calculate the  $S_{v,G}$ , and  $S_{v,SG}$  based on equations (3) and (5) since these grades exhibit elongated grains. And the  $S_{v,G}$ , and  $S_{v,SG}$  of W-RX, W1TiC, and W2YO, which exhibit equiaxed grains, are calculated using equations (4) and (5) where the  $S_{v,G}$  and  $S_{v,tG}$  can be calculated from the HAGBs D50 (as shown in table 2) and D50 with the misorientation angle larger than  $2^\circ$  (W-RX:  $59.3 \mu\text{m}$ ; W1TiC:  $5.7 \mu\text{m}$ ; W2YO:  $5.9 \mu\text{m}$ ), respectively. Equation (6) is applied to calculate the  $S_{v,p}$  for the particle reinforced tungsten (W0.5ZrC, W1TiC, and W2YO). The calculated  $S_{v,G}$ ,  $S_{v,SG}$ , and  $S_{v,p}$  of various tungsten grades are summarized in figure 5.

Particle reinforced tungsten grades exhibit high total boundary surface area to volume ratio  $S_{v,total}$  (the sum of  $S_{v,G}$ ,  $S_{v,SG}$ , and  $S_{v,p}$ ) apparently because of the small strengthening particles embedded in the tungsten matrix. The strengthening particles suppress grain growth (during sintering) helping to keep grain size small in comparison with the commercial tungsten grades. W0.5ZrC grade has the highest  $S_{v,G}$  and  $S_{v,p}$  among other tungsten grades because it has the smallest grain size and particle size, which is also reported in the earlier study [9].

The  $S_{v,SG}$  (i.e. the density of LAGBs) of IGP, IGA, and W0.5ZrC grades is much larger than the one of W1TiC and W2YO materials. This is expected since W1TiC and W2YO are produced using the PIM process, which applies sintering at a temperature higher than  $2000^\circ\text{C}$  [7] without any further

mechanical processing such as rolling or forging. As a result, the LAGB density of W1TiC and W2YO is lower than that of the rolled or hammered tungsten grades.

Respectively, the W0.5ZrC and W-RX grades exhibit the highest and lowest  $S_{v,total}$  among the studied products. The low  $S_{v,total}$  of W-RX is clearly an outcome of the recrystallization process, keeping in mind that before the annealing, the IGP had a very high  $S_{v,SG}$ , being one of the driving forces for the recrystallization process. During the recrystallization process, the LAGBs sweep across the grains and thereby getting removed. As a result, large grains with a high misorientation angles are formed.

### 3.2. Vickers hardness and irradiation hardening

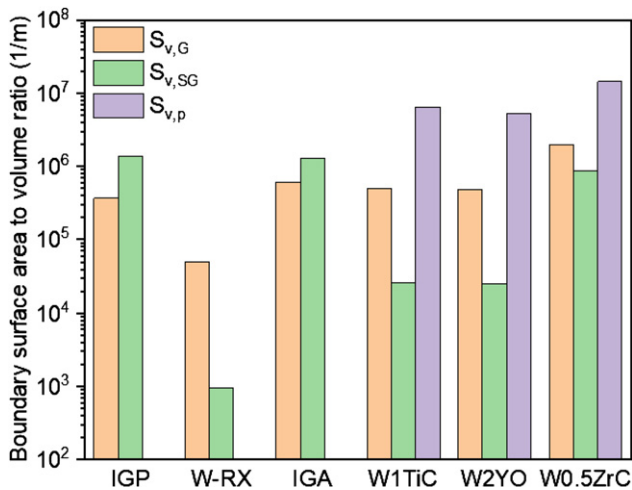
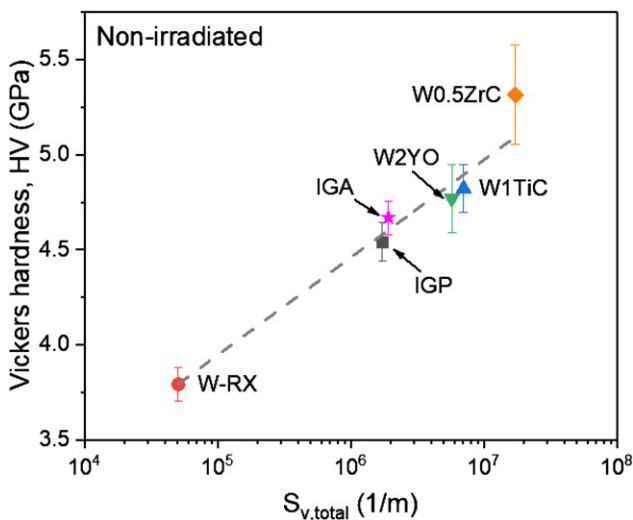
As shown in figure 6, the hardness of non-irradiated tungsten grades varies as a logarithmic function of  $S_{v,total}$ . As discussed above, the boundaries act as obstacles or barriers, restraining the mobility of dislocations. Therefore, W0.5ZrC has the highest hardness because of the excessively high  $S_{v,total}$ . Besides the grain boundary and strengthening particles, the bulk dislocation lines and networks also contribute to the hardness [20]. As reported by Dubinko, *et al* [32], the dislocation density of W0.5ZrC is around  $10^{13} \text{ m}^{-2}$ , which is higher than the dislocation density of IGP ( $4.2 \times 10^{12} \text{ m}^{-2}$ ) and W2YO ( $2.4 \times 10^{12} \text{ m}^{-2}$ ). This could explain why the average hardness of W0.5ZrC seems to be higher than the grey trendline, even though the trendline crosses the error bar.

The neutron irradiation hardening and the ratio of irradiation hardening to Vicker hardness for the non-irradiated state of the various tungsten grades are shown in figure 7. For all the investigated tungsten grades, except for W0.5ZrC, the irradiation hardening increases as the irradiation temperature ( $T_{irr}$ ) goes from  $600^\circ\text{C}$  up to  $1000^\circ\text{C}$ . However, for W0.5ZrC (as reported in our recent work [18]), the irradiation hardening at  $600^\circ\text{C}$  is similar to that at  $T_{irr} = 1000^\circ\text{C}$ . It might be the result of the high sink strength (i.e. high  $S_{v,total}$ ), which offers better resistance to irradiation (i.e. lower increase of the hardness) by reducing the accumulation of damage, as will be discussed below.

With the exception of W1TiC, all tungsten grades exhibit a decrease of the irradiation hardening as the irradiation temperature rises from  $1000^\circ\text{C}$  to  $1200^\circ\text{C}$ . The reduction of the irradiation hardening can be the result of the annihilation of irradiation-induced defects and possibly recrystallization/recovery taking place simultaneously. For W1TiC, W2YO, and W-RX, only the annihilation of irradiation-induced defects is expected as these grades must be resistant to recrystallization up to  $1200^\circ\text{C}$  and even up to higher temperatures. The reason for the resistance of the PIM grades comes from the fabrication, as the sintering was performed at very high temperature (up to  $2000^\circ\text{C}$ ). W-RX has already been recrystallized at  $1600^\circ\text{C}$  for 1 h. Thus, these materials exhibit extremely low dislocation/LAGBs density, which is the driving force for the recrystallization process in as-fabricated ITER specification tungsten [32]. Moreover, the strengthening particles in the PIM tungsten grades can restrain the movement of grain boundaries [7]. However, the W1TiC material does

**Table 3.** The medium length of the major and minor axes of grains of IGP, IGA, and W0.5ZrC products.

Materials	Medium length ( $\mu\text{m}$ )							
	Grains or sub-grains with misorientation $> 2^\circ$				Grains with HAGBs			
	A	B <sub>1</sub>	B <sub>2</sub>	C	A	B <sub>1</sub>	B <sub>2</sub>	C
<b>IGP</b>	3.9	1.6	2.0	1.2	77.1	10.0	12.5	4.8
<b>IGA</b>	2.5	1.4	2.0	1.1	15.6	5.7	8.1	2.9
<b>W0.5ZrC</b>	1.7	0.9	1.4	0.8	5.1	1.7	1.9	1.0

**Figure 5.** Boundary surface area to volume ratio of HAGBs ( $S_{v,G}$ ), LAGBs ( $S_{v,SG}$ ), and particle ( $S_{v,p}$ ) of the studied tungsten grades.**Figure 6.** Relationship between total boundary surface to volume ratio and Vickers hardness value.

not involve the annihilation of irradiation-induced defects, as the hardness increases with increasing irradiation temperature. The absence of the reduction of the irradiation hardening in W1TiC requires further investigation. Differently from the PIM particle reinforced grades and W-RX, IGP and IGA have a high density of LAGBs, higher density of bulk dislocations, and do not contain strengthening particles. As indicated by

Pintsuk, *et al* [19] and Tsuchida, *et al* [33], both IGP and IGA will be recrystallized up on long-term thermal exposure at a temperature of 1200 °C. Although W0.5ZrC also contains high LAGBs density (shown in figure 5), the resistance against the recrystallization is known to be higher than that of the rolled pure tungsten [9]. Therefore, the combined effect of irradiation enhanced and thermally assisted recrystallization (reduction of dislocation density, reduction of LAGBs density, nucleation of new grains with an equiaxed shape) on the resulting hardness is expected to play a role in the case of the commercial tungsten grades i.e. IGP and IGA, while the microstructure of the particle reinforced materials is expected to be stable against thermal exposure during irradiation. Although the hardness measured after irradiation at 1200 °C is lower than the one at the other two irradiation temperatures (except for W1TiC), the hardness after irradiation at 1200 °C still rises by 30%–60% compared to the reference value, as shown in figure 7(b). In other words, the annihilation of irradiation-induced defects does not fully suppress the accumulation of irradiation-induced defects at 1200 °C (roughly one-third of the melting point of tungsten).

Additional experimental data on the neutron irradiation hardening taken from the literature [12, 14, 34, 35] for two different tungsten materials irradiated in HFIR and JOYO are also added on figure 7. The grade irradiated in HFIR is the hot rolled pure tungsten annealed at 1300 °C for 1 h, and the grade irradiated in JOYO is from an arc-melted pure tungsten ingot annealed at 1400 °C for 1 h [12]. Although the grain properties of these two types of tungsten are unknown, their  $S_{v,G}$  and  $S_{v,SG}$  are expected to be similar to W-RX because of the annealing process. With a similar dose ( $\sim 1$  dpa), the irradiation hardening resulting from the irradiation in HFIR and JOYO reactors is around two times higher than the one measured after the irradiation in BR2. Three possible reasons can be put forward to explain this difference. Firstly, since the irradiation at HFIR was performed in the flux trap channel, the ratio of thermal to fast neutron flux was very high. In the case of BR2 irradiation, the specimens were placed directly inside the fuel element to reduce thermal to fast ratio as much as possible, and a thick stainless steel wall is used to absorb thermal neutrons coming from other fuel elements. As a result, the calculated concentration of the transmuted element (Re and Os) in the HFIR irradiation [12] is higher than the one in BR2. Large amount of precipitation has been observed in the HFIR irradiation specimens, which is a result of the high concentration of transmuted elements [12]. And, within all types of irradiation-induced defects, precipitation has the highest contribution to

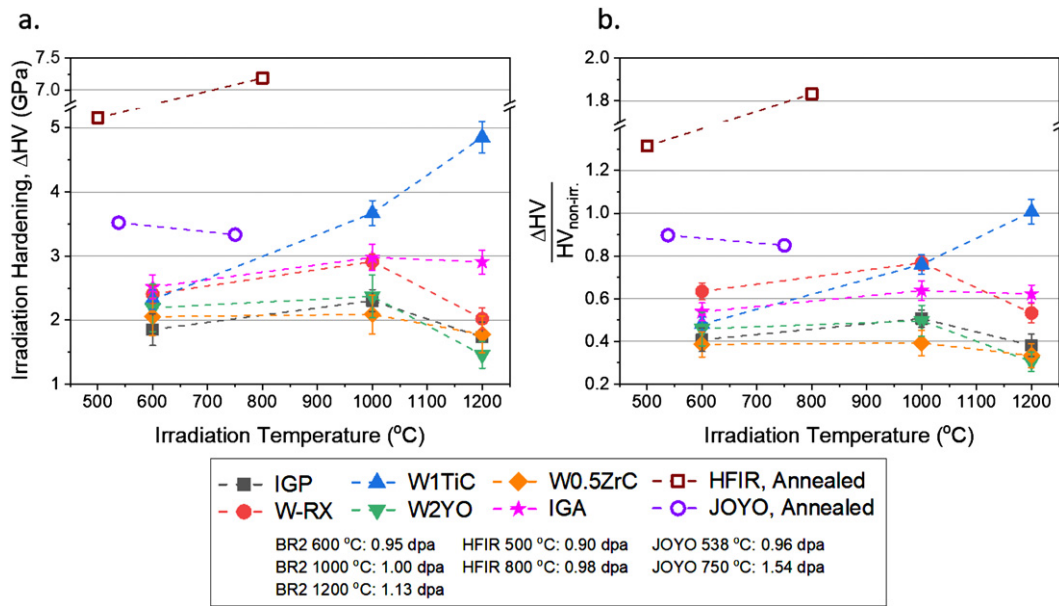


**Figure 7.** (a) Neutron irradiation hardening and (b) ratio of irradiation hardening to nominal hardness as a function of irradiation temperature. The results for the irradiation campaigns at HFIR and JOYO reactors are taken from the literature (HFIR 500 °C 0.90 dpa [14], HFIR 800 °C 0.98 dpa [12], JOYO 538 °C 0.96 dpa [34], JOYO 750 °C 1.54 dpa [35]). The results of W0.5ZrC, W-RX, and IGA are taken from our recent work [18].

hardening [17], which is the reason why the irradiation hardness of HFIR is larger than the one of BR2 irradiated materials. Secondly, as reported by Hasegawa *et al* [12], the specimens irradiated in JOYO reactor are fabricated from the arc-melted ingot annealed at 1400 °C for 1 h. Therefore, these specimens are expected to have a large grain size. Since their grain size is larger than most of the specimens' grain size studied in this work, more irradiation-induced defects (voids and dislocation loops) are expected to form (due to the effect of the sinking at grain boundaries [36]). Thirdly, the dose rate of JOYO is higher than for both BR2 and HFIR. Given a higher dose rate, the irradiation time to reach an equivalent dose is shorter for the irradiation in JOYO reactor. As the irradiation dose rate increases, the lattice defects (Frenkel pairs and defect clusters) are injected more frequently while their diffusion coefficients (controlling the rate at which defects reach static sinks) remain constant given constant irradiation temperature [37]. As a result, under higher dose rate, a high concentration of defects becomes available for mutual interaction leading to the formation of larger clusters, turning later into voids and loops. However, the high concentration of stable irradiation defects leads to the lower growth rate, because newly introduced defects are distributed among the sinks and stable irradiation defects [37]. That is the reason why the high irradiation flux has a lower void and dislocation loop growth rate (but high density of those defects) compared to a low irradiation flux. Thus, the neutron irradiation with a higher dose rate results in a larger number density of the irradiation-induced defects of a smaller size, which should introduce a higher hardening effect (mainly driven by the defect density). However, the concentration of transmuted elements after the irradiation in JOYO reactor should be the lowest since it is a fast reactor. Thus, the

combination effect of sink strength, dose rate, and concentration of transmuted elements may explain why the irradiation hardening resulting from the JOYO irradiation is lower compared to the one induced by the irradiation in HFIR reactor but higher than the one in BR2.

Given the currently established understanding of the irradiation damage [36, 37], the irradiation hardening effect is expected to reduce with increasing grain boundary density (i.e. reducing grain size) and phase boundary density (i.e. increasing particle density) because both types of these planar defects are believed to act as sinks for the irradiation defects. It is expected that one-dimensionally and three-dimensionally migrating irradiation defects will get absorbed/ attracted at these planar defects and therefore will not contribute to the formation of voids and dislocation loops inside the grain interior. The latter defects are the main sources of irradiation hardening in the limit of relative low irradiation doses, while the Re/Os transmutation remains low enough. As shown in figure 8, most tungsten grades follow the expected trend, except for the IGP, which has low irradiation hardening although  $S_{v,G}$  is relatively small for this material.

The  $S_{v,SG}$  is not included in this discussion because regular LAGBs have lower sink strength compared to the HAGBs. Indeed, as indicated in the literature [38], a large grain boundary density will promote the formation of nano-voids within the grains because of the anisotropy of the diffusion of self-interstitial atom and of their clusters, which promotes supersaturation of the 3D-migrating vacancies. Thus, the population of the resulting irradiation-induced defects (voids and dislocation loops) depends not only on irradiation dose and temperature but also on sink strength, which is linked to the boundary (and bulk dislocation) density. As shown in figures 5 and 7, IGP has a lower  $S_{v,G}$  compared to the W1TiC, W2YO, and IGA

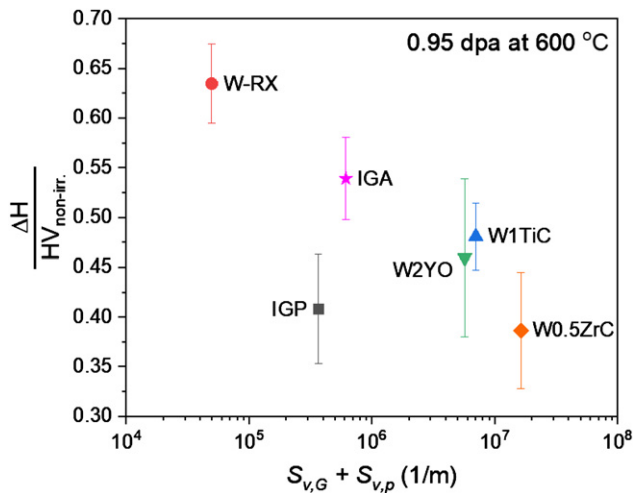


**Figure 8.** Ratio of the irradiation hardening divided by the nominal hardness vs summed grain boundary and particle surface to volume ratio ( $S_{v,G}$  and  $S_{v,p}$ ). The hardness after irradiation of W0.5ZrC, W-RX, and IGA are taken from our recent work [18].

material. Consequently, one should expect the void density established in the IGP to be lower than that in other tungsten grades. If that is indeed the case, and since the voids have a larger contribution to the hardening compared to the dislocation loops in tungsten [17], the irradiation hardening in the IGP should indeed be lower. Thus, grain refinement, required to achieve high strength and low DBTT in the non-irradiated material, might have a counter-productive effect in terms of the preferential formation of the voids yielding to the irradiation hardness and subsequent embrittlement. Unlike the pure tungsten grades, W1TiC, W2YO, and W0.5ZrC have strengthening particles that provide phase boundaries as additional sinks. As shown in figure 8, these additional sinks have a positive effect on the resistance against irradiation hardening. This might be explained by the different sink strength and sink bias between grain boundary and phase boundary (difference comes the fact that grain boundaries may absorb dislocation loops, while strengthening particles cannot). Clearly, both of the above discussed hypotheses require further investigation by TEM.

#### 4. Conclusions

The irradiation hardening of several tungsten grades irradiated in the BR2 reactor at 600, 1000, and 1200 °C to  $\sim 1$  dpa has been assessed by parametric hardness measurements performed at room temperature. Based on the experimentally measured hardness, the following conclusions can be made:

- The highest irradiation hardening is reached at 1000 °C in all the tested grades except for W1TiC, which shows an abnormal increase of the irradiation-induced hardness at 1200 °C. Further microstructural investigation is required on this material to understand the reasons for this unexpected result.
- Although the irradiation hardness at  $T_{irr} = 1200$  °C is smaller compared to the one measured at 600 °C and

1000 °C, it is not negligible and actually amounts to about 30%–60% of the reference hardness value. Thus, even at high irradiation temperature ( $T_m/3$ ), the accumulation of irradiation defects in tungsten is not suppressed.

- The smallest irradiation-induced hardness (i.e. best resistance to the irradiation damage) is observed in IGP and W0.5ZrC products at  $T_{irr} = 600$  to 1000 °C, which can be explained by a high density of sinks (i.e. the density of LAGB, HAGB, dislocations, and particles in W0.5ZrC). The evaluation of the irradiation hardness at  $T_{irr} = 1200$  °C requires additional EBSD and TEM analysis of the irradiated samples as certain recrystallization and bulk dislocation recovery may occur during the extended irradiation period (125 days of irradiation).

#### Acknowledgments

This work has been carried out within the framework of the EUROfusion Consortium and has received funding from the Euratom research and training programme 2014–2018 and 2019–2020 under Grant Agreement No. 633053. The views and opinions expressed herein do not necessarily reflect those of the ITER Organization or of the European Commission. The work was partially supported by FOD fusion Grant.

#### ORCID iDs

Marius Wirtz  <https://orcid.org/0000-0002-1857-688X>

#### Reference

- You J.H. et al 2018 European divertor target concepts for DEMO: design rationales and high heat flux performance *Nucl. Mater. Energy* **16** 1–11
- Barrett T.R. et al 2016 Progress in the engineering design and assessment of the European DEMO first wall and divertor plasma facing components *Fusion Eng. Des.* **109–111** 917–24
- Pitts R. et al 2019 Physics basis for the first ITER tungsten divertor *Nucl. Mater. Energy* **20** 1–25
- Yin C. et al 2018 Tensile properties of baseline and advanced tungsten grades for fusion applications *Int. J. Refract. Met. Hard Mater.* **75** 153–62
- Xie Z.M., Zhang T., Liu R., Fang Q.F., Miao S., Wang X.P. and Liu C.S. 2015 Grain growth behavior and mechanical properties of zirconium micro-alloyed and nano-size zirconium carbide dispersion strengthened tungsten alloys *Int. J. Refract. Met. Hard Mater.* **51** 180–7
- Lied P., Bonnekoh C., Pantleon W., Stricker M., Hoffmann A. and Reiser J. 2019 Comparison of K-doped and pure cold-rolled tungsten sheets: as-rolled condition and recrystallization behaviour after isochronal annealing at different temperatures *Int. J. Refract. Met. Hard Mater.* **85** 105047
- Antusch S. et al 2015 Mechanical and microstructural investigations of tungsten and doped tungsten materials produced via powder injection molding *Nucl. Mater. Energy* **3–4** 22–31
- Xie Z.M. et al 2015 Extraordinary high ductility/strength of the interface designed bulk W–ZrC alloy plate at relatively low temperature *Sci. Rep.* **5** 1–11

- [9] Deng H., Xie Z., Wang Y., Liu R., Zhang T., Hao T., Wang X., Fang Q. and Liu C. 2018 Mechanical properties and thermal stability of pure W and W-0.5wt% ZrC alloy manufactured with the same technology *Mater. Sci. Eng. A* **715** 117–25
- [10] Zhang T., Deng H.W., Xie Z.M., Liu R., Yang J.F., Liu C.S., Wang X.P., Fang Q.F. and Xiong Y. 2020 Recent progresses on designing and manufacturing of bulk refractory alloys with high performances based on controlling interfaces *J. Mater. Sci. Technol.* **52** 29–62
- [11] Li M. and You J.-H. 2015 Interpretation of the deep cracking phenomenon of tungsten monoblock targets observed in high-heat-flux fatigue tests at 20 MW m<sup>-2</sup> *Fusion Eng. Des.* **101** 1–8
- [12] Hasegawa A., Fukuda M., Nogami S. and Yabuuchi K. 2014 Neutron irradiation effects on tungsten materials *Fusion Eng. Des.* **89** 1568–72
- [13] Hasegawa A., Fukuda M., Yabuuchi K. and Nogami S. 2016 Neutron irradiation effects on the microstructural development of tungsten and tungsten alloys *J. Nucl. Mater.* **471** 175–83
- [14] Fukuda M., Yabuuchi K., Nogami S., Hasegawa A. and Tanaka T. 2014 Microstructural development of tungsten and tungsten–rhenium alloys due to neutron irradiation in HFIR *J. Nucl. Mater.* **455** 460–3
- [15] Fukuda M., Kiran Kumar N.A.P., Koyanagi T., Garrison L.M., Snead L.L., Katoh Y. and Hasegawa A. 2016 Neutron energy spectrum influence on irradiation hardening and microstructural development of tungsten *J. Nucl. Mater.* **479** 249–54
- [16] Fukuda M., Hasegawa A., Tanno T., Nogami S. and Kurishita H. 2013 Property change of advanced tungsten alloys due to neutron irradiation *J. Nucl. Mater.* **442** S273–6
- [17] Hu X., Koyanagi T., Fukuda M., Kumar N.A.P.K., Snead L.L., Wirth B.D. and Katoh Y. 2016 Irradiation hardening of pure tungsten exposed to neutron irradiation *J. Nucl. Mater.* **480** 235–43
- [18] Terentyev D., Yin C., Dubinko A., Chang C. and You J. 2020 Neutron irradiation hardening across ITER diverter tungsten armor *Int. J. Refract. Met. Hard Mater.* **105** 437
- [19] Pintsuk G., Antusch S., Weingaertner T. and Wirtz M. 2018 Recrystallization and composition dependent thermal fatigue response of different tungsten grades *Int. J. Refract. Met. Hard Mater.* **72** 97–103
- [20] Askeland D.R., Phulé P.P., Wright W.J. and Bhattacharya D. 1996 *The Science and Engineering of Materials* (New York: Springer)
- [21] Klamkin M.S. 1971 Elementary approximations to the area of  $n$ -dimensional ellipsoids *Am. Math. Mon.* **78** 280–3
- [22] Klamkin M.S. 1976 Corrections to elementary approximations to the area of  $N$ -dimensional ellipsoids *Am. Math. Mon.* **83** 478
- [23] Thomsen K. 2004 Surface area of an ellipsoid <https://numerica.com/answer/ellipsoid.htm#thomsen>
- [24] Gaganidze E., Chauhan A., Schneider H.-C., Terentyev D., Borghmans G. and Aktaa J. Fracture-mechanical properties of neutron irradiated ITER specification tungsten *J. Nucl. Mater.* 152761.
- [25] Yin C., Terentyev D., Zhang T., Petrov R.H. and Pardoën T. 2020 Impact of neutron irradiation on the strength and ductility of pure and ZrC reinforced tungsten grades *J. Nucl. Mater.* **537** 152226
- [26] Bonny G. *et al* 2020 Trends in vacancy distribution and hardness of high temperature neutron irradiated single crystal tungsten *Acta Mater.* **198** 1–9
- [27] Pelowitz D. *et al* 2011 *MCNPX 2.7.0 Extensions* (Los Alamos National Laboratory)
- [28] Stankovskiy A., Van den Eynde G. and Fiorito L. 2018 *ALEPH V2.7, A Monte Carlo Burn-Up Code* (SCK•CEN)
- [29] JEFF Scientific Working Group 2017 *The Joint Evaluated Fission and Fusion Nuclear Data Library JEFF-3.3* (Nuclear Energy Agency)
- [30] Brown D.A. *et al* 2018 ENDF/B-VIII.0: the 8th major release of the nuclear reaction data library with CIELO-project cross sections, new standards and thermal scattering data *Nucl. Data Sheets* **148** 1–142
- [31] Konobeyev A.Y., Fischer U., Korovin Y.A. and Simakov S.P. 2017 Evaluation of effective threshold displacement energies and other data required for the calculation of advanced atomic displacement cross-sections *Nucl. Energy Technol.* **3** 169–75
- [32] Dubinko A., Yin C., Terentyev D., Zinovev A., Rieth M., Antusch S., Vilémová M., Matějček J. and Zhang T. 2020 Plastic deformation in advanced tungsten-based alloys for fusion applications studied by mechanical testing and TEM *Int. J. Refract. Met. Hard Mater.* **105** 409
- [33] Tsuchida K., Miyazawa T., Hasegawa A., Nogami S. and Fukuda M. 2018 Recrystallization behavior of hot-rolled pure tungsten and its alloy plates during high-temperature annealing *Nucl. Mater. Energy* **15** 158–63
- [34] Tanno T., Fukuda M., Nogami S. and Hasegawa A. 2011 Microstructure development in neutron irradiated tungsten alloys *Mater. Trans.* **52** 1447
- [35] Tanno T., Hasegawa A., He J.-C., Fujiwara M., Nogami S., Satou M., Shishido T. and Abe K. 2007 Effects of transmutation elements on neutron irradiation hardening of tungsten *Mater. Trans.* **48** 2399
- [36] Golubov S., Singh B. and Trinkaus H. 2000 Defect accumulation in fcc and bcc metals and alloys under cascade damage conditions—towards a generalisation of the production bias model *J. Nucl. Mater.* **276** 78–89
- [37] Was G.S. 2016 *Fundamentals of Radiation Materials Science: Metals and Alloys* (Berlin: Springer)
- [38] Castin N., Bakaev A., Bonny G., Sand A.E., Malerba L. and Terentyev D. 2017 On the onset of void swelling in pure tungsten under neutron irradiation: an object kinetic Monte Carlo approach *J. Nucl. Mater.* **493** 280–93